



Interpreting carbon-water trade-offs in Daisy crop model using Pareto-based calibration Laura Delhez¹, Eric Laloy², Quentin Beauclaire¹, Bernard Longdoz¹

¹Biosystems Dynamics and Exchanges (TERRA Teaching and Research Centre), University of Liège, Gembloux, 5030, Belgium

Abstract. Improving the simulation of carbon and water exchanges is crucial for reliable crop modelling under changing

²Sustainable Waste & Decommissioning, Belgian Nuclear Research Centre (SCK-CEN), Mol, 2400, Belgium *Correspondence to: Laura Delhez (laura.delhez@uliege.be) and Bernard Longdoz (bernard.longdoz@uliege.be)

climate conditions. Although model calibration is a key step, optimising multiple outputs can be challenging and often reveals trade-offs between calibration objectives. We applied a Pareto-based multi-objective calibration with the Speed-constrained Multi-objective Particle Swarm Optimisation (SMPSO) algorithm to the Daisy soil–plant–atmosphere model, targeting dry matter (DM), net ecosystem exchange (NEE), and latent heat flux (LE) of winter wheat crops.

The optimal parameter set achieved good accuracy for all objectives (RMSE = $0.948 \, t \, ha^{-1}$ for DM, $1.49 \, gC \, m^{-2} \, day^{-1}$ for daily NEE and $30.7 \, W \, m^{-2}$ for daily LE) but revealed singular trade-offs. The strong compromise between dry matter and NEE likely suggests wrong parameterisation and measurement bias, while the trade-off between NEE and LE reflects equifinality issues from evapotranspiration partitioning. Lastly, this analysis also pointed out limitations in simulating stomatal regulation during heatwaves conditions, supporting the decoupling between transpiration and carbon assimilation. These findings show that Pareto-based calibration can also serve as a diagnostic tool, identifying structural weaknesses and guiding targeted improvements in process representation for more robust crop model evaluation.

1 Introduction

20 Crop models are essential tools for yield forecasting and decision-making, but also for assessing the impact of climate change and understanding the complex interactions within the soil-plant-atmosphere continuum (Asseng et al., 2019). Over recent decades, they have been actively developed to account for changing environmental conditions such as rising temperature and elevated atmospheric CO₂ (Timlin et al., 2024). As a result, crop models now integrate more complex approaches and detailed processes, replacing for instance the tipping-bucket approach with Richard's equation for soil water dynamics, or using biochemical photosynthesis models (Farquhar et al., 2001) instead of radiation-use efficiency. Biochemical models are often coupled with stomatal conductance models to jointly simulate CO₂ and water fluxes (Keenan et al., 2010). Such couplings are now implemented in advanced crop models such as GECROS (Yin and van Laar, 2005) and Daisy (Plauborg et al., 2010) as well as in most terrestrial biosphere models (e.g. SiB2, ORCHIDEE, IBIS, JULES, etc.). These biosphere models have also been combined with crop models in order to improve crop development and yield predictions while accurately simulating gas exchanges. Few examples are SiBcrop (Lokupitiya et al., 2009), ORCHIDEE–STICS (de Noblet-Ducoudré et al., 2004), Agro–IBIS (Kucharik, 2003) and JULES–SUCROS (Van den Hoof et al., 2011).





In these couplings, carbon and water fluxes between vegetation and atmosphere are assumed to only be regulated by stomatal behaviour. When water is not limiting, plants open their stomata in order to maximise their carbon uptake. Conversely, they reduce their stomatal aperture under water stressed conditions, compromising between carbon assimilation and water loss (Manzoni et al., 2011). This response is often represented by a decrease of g_1 , the slope parameter connecting stomatal conductance to carbon assimilation (Zhou et al., 2013; Liu et al., 2009). Nevertheless, as stomatal behaviour is influenced by multiple drivers (soil water status, atmospheric dryness, leaf temperature ...) which often co-exist during extreme events such as droughts or heatwaves, plant responses may sometimes be contradictory (Grossiord et al., 2020). To date, these complex interactions remain poorly understood and insufficiently represented in models (Liu K. et al., 2024; Sabot et al., 2022).

In this context, where stomatal behaviour controls both carbon assimilation and water loss, model calibration requires simultaneous assessment of different outputs. Calibrating against a single output (e.g. evapotranspiration) can result in compensating errors or masking structural deficiencies (Cameron et al., 2022). Multi-objective calibration therefore provides a well-suited framework, although it presents a significant challenge due to the high-dimensional parameter space of such models, the large computational cost of search algorithms and the potentially conflicting nature of targeted objectives.

Extensively used in calibration of hydrological models (e.g., Efstratiadis and Koutsoyiannis, 2010; Jahandideh-Tehrani et al., 2020, Moges et al., 2020), Multi-Objective Optimisation (MOO) algorithms aim at optimising all objectives simultaneously and explicitly handle conflicting objectives by exploring trade-offs using a Pareto-based sampling approach (Sharma and Kumar, 2022). This method allows modellers to select any points on the Pareto front, i.e. select an optimal parameter set depending on the modeller's preference (Tang et al., 2018).

Beyond identifying optimal parameter sets, Pareto-based calibration can also provide valuable insights into model behaviour. It can help detect ill-posed models, revealing structural inadequacies, missing processes or equifinality (Kollat et al., 2012; Efstratiadis and Koutsoyiannis, 2010). Recently, Harvey et al. (2023) analysed the change of the Pareto front solutions between calibration and validation sets, pointing out the influence of data type and model structure. Another study used Pareto-optimal solutions as informative priors to guide posterior uncertainty estimation within a Bayesian framework (Tang et al., 2018).

In this case study, five growing seasons of winter wheat, cultivated on a Belgian site, were simulated using Daisy soil–plant–atmosphere model (Plauborg et al., 2010). We applied a swarm-based MOO algorithm called Speed-constrained Multi-objective Particle Swarm Optimisation (SMPSO) targeting three outputs: dry matter of vegetation organs (DM), Net CO₂ Ecosystem Exchange (NEE) and latent heat flux (LE). The last two variables capture the coupling between carbon and water cycles, whereas NEE and DM (considering carbon as a known fraction) are essential for assessing the crop carbon budget. By calibrating against these three outputs, our objectives were to improve model performance as well as to explore the trade-offs between them, revealing potential issues such as structural shortcomings or equifinality.





2 Materials and methods

2.1. Case study

The study site is a 12 ha cropland located in Lonzée, Belgium, with a temperate maritime climate ($\overline{T} = 11.1^{\circ}C$ and annual precipitation of 716 mm). Cultivated for more than 85 years on a silt loam soil, this site is equipped with an eddy covariance system and a micrometeorological station since 2004, as a part of the Fluxnet network. Since 2017, this monitoring site has integrated the ICOS network as a Level 2 station named BE-Lon (https://www.icos-cp.eu/).

This study focuses on five growing seasons of winter wheat (Triticum asstinum L.) which are summerised in Table 1. Sown in

This study focuses on five growing seasons of winter wheat (*Triticum aestivum L*.) which are summarised in Table 1. Sown in late October, TOB and SKY varieties are known to reach heading and maturity stages faster than SAH and SMA cultivars (Meza et al., 2018; 2023). As the same cultivar was sown for VAL and SAH, VAL season was set aside for the validation. During these five seasons, regular measurements of biomass were performed along with continuous measurements of NEE and LE. These flux data were corrected for frequency losses and filtered for low turbulence and nonstationary conditions, contributing to high-quality coverages detailed in Table 1. Flux data treatment is described in De Ligne et al. (2010) and Pastorello et al. (2020). Data collection (fluxes, biomass and soil) as well as additional information on the site, measurements or management activities can be found in Delhez et al. (2025).

Table 1: Summary of winter wheat crops in BE-Lon. Coverage of NEE and LE corresponds to the fraction of high-quality hourly data during the calibration period.

	VAL	SAH	TOB	SMA	SKY
Variety	Sahara	Sahara	Tobak	KWS Smart	LG Skyscraper
Sowing – Harvest	14 Oct 10 – 16 Aug 11	14 Oct 14 – 2 Aug 15	29 Oct 16 – 30 Jul 17	10 Oct 18 – 1 Aug 19	28 Oct 21 – 24 Jul 22
Anthesis (± 5 days)	10 Jun 11	28 Jun 15	15 Jun 17	12 Jun 19	9 Jun 22
Grain yield (t ha ⁻¹)	9.16	8.81	8.63	9.71	11.31
Studied period	1 Mar 10 – 31 Jul 11	1 Mar 14 – 4 Aug 15	1 Mar 16 – 2 Aug 17	1 Mar 19 – 3 Aug 19	1 Mar 22 – 24 Jul 22
Measured dry	Vegetative (leaf+stem),	Vegetative (leaf+stem),	Leaf, stem, storage	Leaf, stem, storage	Leaf, stem, root,
matter	storage organ	storage organ	organ	organ	storage organ
NEE coverage (%)	45.7	46.9	42.6	34.2	47.9
LE coverage (%)	51.0	58.4	61.7	45.7	63.0





80 2.2 Daisy model

90

105

110

2.2.1 Model description and set-up

Daisy is a crop process-based model simulating carbon, nitrogen and water cycles of the soil-vegetation-atmosphere continuum. Initially published by Hansen et al. (1991), Daisy has since been extensively described (Abrahamsen and Hansen, 2000; Hansen et al., 2012), developed (Plauborg et al., 2010; Holbak et al., 2021), evaluated and compared (Palosuo et al., 2011; Tenreiro et al., 2020; Yin et al., 2020) in the literature. Different modelling options are included in Daisy and must be selected by the modeller depending on its objectives and data availability.

In the present study, the 1D version of Daisy was used with an hourly time resolution. Hourly measurements of air temperature, air vapour pressure, global radiation, wind strength and precipitation were provided as inputs. Water movement in unsaturated soil is described by Richard's equation and, for each soil layer, retention and conductivity curves have been established with the Mualem–van Genuchten model (Mualem, 1976; van Genuchten, 1980). Below the soil profile, there is an aquitard layer (i.e., water blocking layer) and an aquifer whose pressure varies according to water table depth measurements also provided as inputs. Potential evapotranspiration is estimated with the FAO56 Penman-Monteith equation, using the reference evapotranspiration (ET0) adjusted to surface cover through bare soil and crop coefficients (Allen et al., 1998; 2006). Water can be evaporated from free water surfaces (canopy interception or ponding), from soil surface or transpired by plants. Actual soil evaporation is governed by the soil hydraulic conductivity, as soil water must be transported to the soil surface. As for the actual transpiration, it is computed together with the entire surface energy balance within the soil—vegetation—atmosphere transfer (SVAT) module (Plauborg et al., 2010). To solve numerically this energy balance, the SVAT module is coupled with the biochemical photosynthesis model of de Pury and Farquhar (1997) and a stomatal conductance empirical model (Leuning, 1995). In this version, the stomatal conductance g_s is adjusted to account for hydraulic signalling (Plauborg et al., 2010):

$$100 g_s = g_0 + \frac{g_1 \cdot e^{-\delta|\psi_c|}}{\left(1 + \frac{VPD}{D_0}\right) \cdot (C_s - \Gamma)} A_{net}, (1)$$

where A_{net} is the net leaf CO₂ assimilation rate, C_s is the CO₂ concentration at the leaf surface, Γ is the CO₂ compensation point, VPD is the vapour pressure deficit, ψ_c is the crown water potential (with the related parameter δ) and g_0 , g_1 and D_0 are Leuning parameters.

Compared to Daisy v7.0.7, several modifications related to the diffuse radiation, maintenance respiration and carbon reserve remobilisation were made (Appendix A) and later integrated in the latest version (v7.1.0).

2.2.2 Model parameters

In their global sensitivity analysis performed on yield, NEE and LE, Delhez et al. (2025) demonstrated the significant influence of about 25 parameters out of 200. However, some adjustments to their selection have made for this present work. The influential parameters related to the phenology, the allocation and the diffuse fraction of radiation have already been estimated separately, as direct measurements are carried out at BE-Lon station. Additionally, the temperature scaling constant $c_{-}Vm$ and





the leaf RuBisCO-N fraction were discarded and set to their default value because of their high correlation with other parameters. Conversely, some parameters were added as this study takes new processes into account, such as the photosynthetic contribution of stem and storage organs. Hence, there are 22 parameters included in this study, all described in Table 2.

Table 2: Model parameters used in this study and their acceptable range.

Parameter	Range ^b	Units	Description Fraction of PAR effectively absorbed by PSII (in Daisy: alfa)		
f PSII a	0.16 - 0.5	-			
Xn^{a}	0.002 - 0.0006	mol mol ⁻¹ s ⁻¹	Ratio of photosynthetic capacity Vmax to leaf RubisCO-N		
${D_0}^{ m a}$	500 - 3500	Pa	Leuning empirical coefficient		
${g_1}^{ m a}$	9 - 18	-	Leuning stomatal slope (in Daisy: m)		
${\cal g_0}^{ m a}$	0.008 - 0.02	mol m ⁻² s ⁻¹	Leuning stomatal intercept (in Daisy: b)		
$\delta^{\scriptscriptstyle a}$	0 - 1	-	Empirical constant for hydraulic signalling		
$SpLAI^a$	0.0144 - 0.0216	$m^2 g^{-1}$	Specific leaf area		
ShldResC ^a	20 – 50	%	Capacity of shielded reserves as fraction of stem dr		
$NNI_{crit}{}^{a}$	1.26 - 1.54	-	Stem/leaf partitioning modifier (threshold)		
$SOrgPhotEff^{a}$	0 - 1	-	Photosynthetic efficiency of storage organ		
$StemPhotEff^a$	0 - 1	-	Photosynthetic efficiency of stem		
PenPar2	0 - 5	°C	Root penetration rate parameter (threshold)		
σ_{NIR}	0.72 - 0.95	-	Leaf scattering coefficient of NIR		
$arepsilon_{leaf}$	0.94 - 0.99	-	Leaf emissivity for longwave radiation		
k_{net}	0.3 - 0.5	-	Radiation extinction coefficient		
A_{brunt}	0.5 - 0.57	-	Brunt parameter (offset)		
B_{brunt}	0.065 - 0.075	hPa ^{-1/2}	Brunt parameter (vapour pressure factor)		
Ke	0.4 - 0.7	-	Conversion of ET0 to bare soil evap. (in Daisy:		
			EpFactor)		
Kc	1 - 1.4	-	Conversion of ET0 to crop transp. (in Daisy: EpFac)		
$K_{sat,1}$	0.01 - 0.05	cm h-1	Hydraulic conductivity at saturation of first soil layer		
$K_{aquitard}$	0.005 - 0.05	cm h ⁻¹	Hydraulic conductivity at saturation of the aquitard		
$Z_{aquitard}$	1 - 2.5	m	Thickness of the aquitard		

^a Parameter estimated separately for each growing season (cultivar-specific).





^b The acceptable ranges were established from measurements, literature and Daisy reference manual.

2.3 Multi-objective calibration

2.3.1 Key concepts

Calibrating model parameters while considering multiple objectives simultaneously can be formulated as a minimisation problem (Eq. 2):

$$\min F(\mathbf{x}) = \begin{bmatrix} F_1(\mathbf{x}) \\ F_2(\mathbf{x}) \\ F_3(\mathbf{x}) \end{bmatrix}, \tag{2}$$

where \mathbf{x} is a vector of model parameters to be optimised and F_i represents the objective functions. In this study, the objective functions correspond to the relative root mean square error (rRMSE) between modelled and observed values (Eq. 3):

$$F_i(\mathbf{x}) = \frac{\sqrt{\frac{1}{n} \sum_{k=1}^{n} (y_k - d_k)^2}}{\frac{1}{n} \sum_{k=1}^{n} d_k},$$
(3)

Here, y_k and d_k denote the modelled and observed values at time step k for DM (i=1), NEE (i=2) and LE (i=3). Normalising the RMSE by the mean of observed data in Eq. 3 enables fair comparison across variables of different scales. As these objectives can be conflicting, the minimisation problem defined in Eq. (2) typically results in a set of trade-off solutions known as the Pareto-optimal set, rather than a single solution (Deb, 2001). In this set, improving one objective cannot occur without degrading at least one of the others. For this reason, these solutions are also referred to as non-dominated solutions. Visualising these non-dominated solutions in the objective space, referred to as the Pareto front, helps to assess the relationship among objectives and identify model structural errors (Efstratiadis and Koutsoyiannis, 2010).

2.3.2 Search algorithm – SMPSO

135

Particle Swarm Optimisation (PSO) is a population-based optimisation technique inspired by the social behaviour of birds within a flock (Kennedy and Eberhart, 1995). Each potential solution, called a particle i, is characterised by its position and velocity, and a swarm is defined as the population of solutions. Aiming to minimise the objective, the particle moves through the search space, balancing between individual exploration (its own experience) and social learning from the swarm (Sharma and Kumar, 2022). The updated position of a particle $\vec{x}_i^{(t+1)}$ is determined by Eq. (4):

$$\vec{x}_i^{(t+1)} = \vec{x}_i^{(t)} + \vec{v}_i^{(t+1)},$$
 (4)

where $\vec{v_i}^{(t+1)}$ is the updated velocity which explicitly expresses the balance between personal and social learning:

140
$$\vec{v}_i^{(t+1)} = w \vec{v}_i^{(t)} + c_1 r_1 \left(\vec{x}_{p_i} - \vec{x}_i^{(t)} \right) + c_2 r_2 \left(\vec{x}_{g_i} - \vec{x}_i^{(t)} \right),$$
 (5)



145

150

155



In Eq. (5), \vec{x}_{p_i} is the best position that particle i has visited, \vec{x}_{g_i} is the best position that the entire swarm has visited (leader), w is the inertia weight controlling the influence of past velocities, r_1 and r_2 are random numbers drawn from the uniform distribution U(0,1), and c_1 and c_2 are learning factors determining the relative influence of personal and global experience. In this study, we employed the Speed-constrained Multi-objective Particle Swarm Optimisation (SMPSO) algorithm, which is specifically designed for multi-objective problems (Nebro et al., 2009). Based on OMOPSO algorithm (Sierra and Coello Coello, 2005), SMPSO also uses Pareto dominance (Sect. 2.3.1) and a crowding factor to identify non-dominated solutions. Moreover, it includes a velocity constriction mechanism to prevent the so-called swarm explosion effect, an external archive to store these non-dominated solutions, and the use of polynomial mutation. As suggested by Nebro et al. (2009), the learning factors c_1 and c_2 were drawn from the distribution U(1.5, 2.5) and the mutation probability was set as the inverse of the problem's dimensionality.

2.3.3 Application

The Python-based framework for MOO called jMetalPy (Benítez-Hidalgo et al., 2019) includes SMPSO algorithm and was used in combination with PyDaisy library. For each parameter sets (i.e. potential solution) generated by SMPSO, the parameter values were transcribed into Daisy setup files, and the model was executed four times, once for each growing season. The three objective functions (rRMSE) were then computed from these four runs and passed back to SMPSO algorithm. Throughout the optimisation process, the hypervolume indicator (referred to as the size of the dominated space) was estimated to evaluate the performance of SMPSO and check for convergence (Guerreiro et al., 2021; Shang et al., 2021). In total, 50000 model simulations were performed with a swam size of 200.

2.4 Validation

As mentioned in Sect. 2.1, VAL growing season was not used for this multi-objective calibration but kept for validation. Parameter sets were selected from the Pareto front established with SMPSO algorithm, and cultivar-specific parameters were taken from SAH season as the same cultivar was sown during both seasons. In order to evaluate the performance of Daisy model, four criteria were estimated: (i) the RMSE expressed in the same units as the variable of interest, (ii) the rRMSE for comparison with the calibration results, (iii) the Normalised Mean Error (NME) revealing bias and (iv) the model efficiency (EF) which is easily interpreted. This last criterion is also known as Nash–Sutcliffe Efficiency coefficient (NSE) and is computed as follows:

$$EF = 1 - \frac{\sum_{k=1}^{n} (y_k - d_k)^2}{\sum_{k=1}^{n} (d_k - \overline{d_k})^2},$$
(6)

In Eq. 6, y_k and d_k denote the modelled and observed values at time step k, and $\overline{d_k}$ is the mean observed value. If the model is perfect, EF = 1, and the validation results are considered acceptable if EF is greater than 0.5 (Dumont et al., 2014).





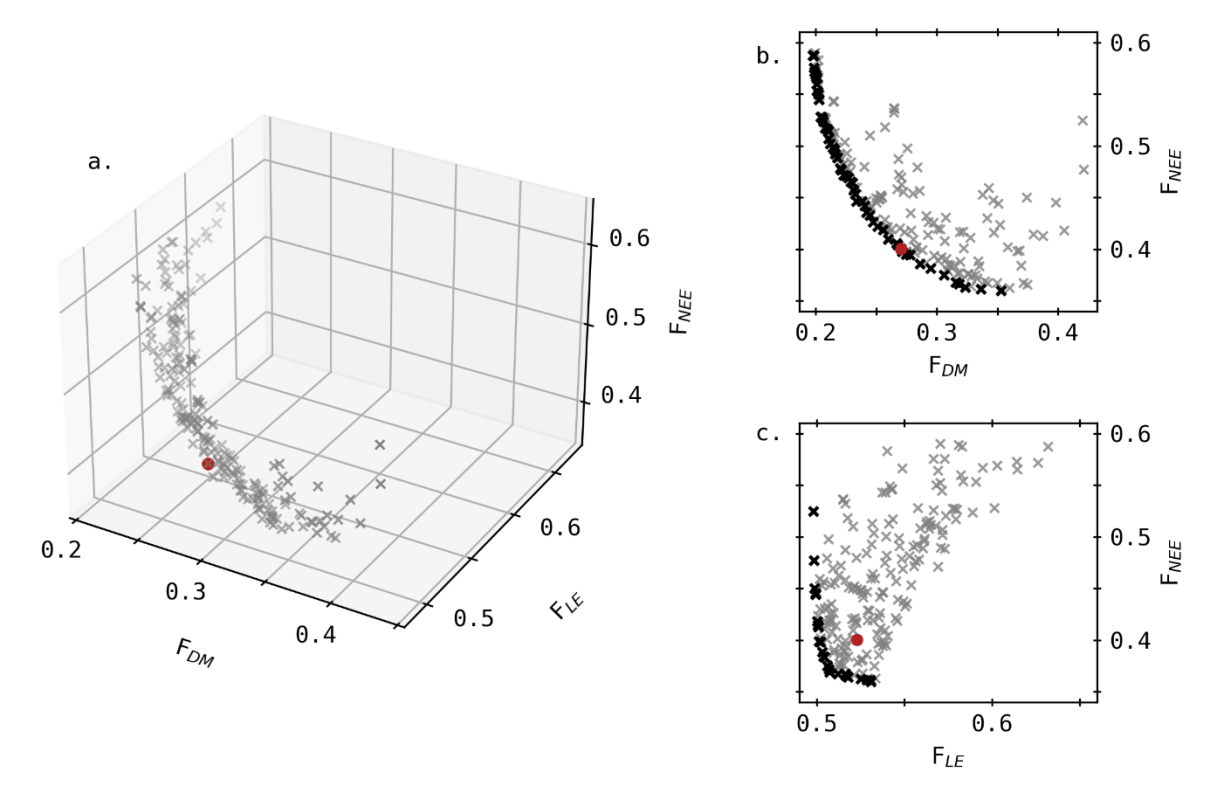
3 Results

175

185

3.1 Pareto front

Non-dominated solutions based on the three objective functions are depicted in Fig. 1a. The red point indicates the most balanced compromise, defined as the non-dominated solution nearest to the point representing the lowest values across all objectives. The trade-off between DM and NEE is the most clearly defined, as shown in the 2D projection (Fig. 1b), where the curved Pareto front extends over a large part of the objective space and most solutions lie along it. Conversely, the LE–NEE front appears angular and narrower, particularly along the LE axis (Figure 1c). Combined with the relatively high rRMSE, it highlights the difficulty in accurately simulating observed LE as well as the limited model responsiveness for this objective.



180 Figure 1: Non-dominated solutions in the objective space: (a) 3D Pareto front according to the rRMSE of DM, LE and NEE, and 2D projection of these solutions considering (b) DM and NEE, (c) LE and NEE. Black dots indicate the Pareto front in 2D space and the red point highlights the most balanced compromise.

Values of the most balanced parameter set (i.e. red point) can be found in Table B1. In Fig. 1a, the specific coordinates of this point are (0.27, 0.40, 0.52) which correspond to RMSE values of 0.948 t ha^{-1} , 3.44 μ mol $m^{-2}s^{-1}$ and 62.7 W m^{-2} for DM, NEE and LE respectively, computed across all four growing seasons. In the following sections, the simulated outputs using this parameter set are compared to observed values in terms of dry matter as well as carbon and water fluxes.



190

195

200



3.2 Dry matter

In addition to the biomass of individual simulated organs (leaf, stem, storage organs SOrg and root), the aboveground vegetative biomass (leaf+stem) was also included in Fig. 2 as distinct measurements of these two organs were not systematic (Table 1). Overall, the simulated dry matter aligns relatively well with observations. Nevertheless, SOrg biomass is consistently underestimated at the end of all growing seasons, resulting in a lower simulated crop yield.

For SAH growing season, this underestimation may be attributed to insufficient remobilisation of stem reserves, as indicated by the high simulated stem biomass in July, even greater than the combined leaf and stem observations. However, this explanation does not hold for the other seasons, where stem biomass appears realistic. Beyond the capacity of remobilised reserves, parameters such as the efficiency of this remobilisation (considered fixed in Daisy) as well as contributions from stem and ear to photosynthesis (SOrgPhotEff and StemPhotEff) may also affect SOrg biomass during the reproductive stage (after anthesis).

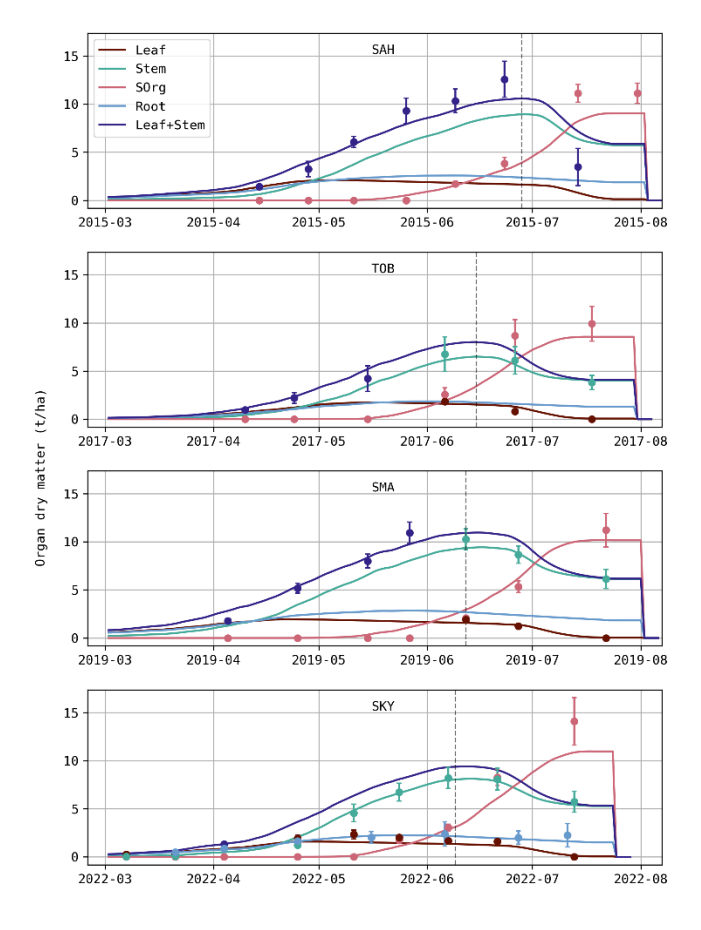


Figure 2: Daily evolution of predicted (solid line) and observed (dot) dry matter for each organ (t ha⁻¹). Error bars depicted for the observed dry matter represent the standard deviations and the dashed vertical line indicates the anthesis.





3.3 Fluxes

205

210

215

As depicted in Fig. 3, the model reproduces the daily dynamics of NEE with good overall agreement. Simulated temporal variations generally follow observed trends, although predictions tend to be more negative (i.e. more CO_2 uptake) during the vegetative stage. This underestimation is particularly evident for TOB growing season, also highlighted by the scatter plot, where the regression slope is significantly higher than 1 ($\beta = 1.14$). This bias suggests either an overestimation of photosynthesis and/or an underestimation of respiration. Despite this discrepancy, the model accurately simulates the biomass of vegetative organs during this stage. On the other hand, during the reproductive stage (when *SOrg* is underestimated; Fig. 2), NEE predictions no longer show a clear bias. This partly explains the observed trade-off between DM and NEE (Fig. 1b). For instance, increasing the remobilisation of stem reserves during SAH would likely result in a more accurate crop yield, but also in an increase in NEE as CO_2 is released through this process.

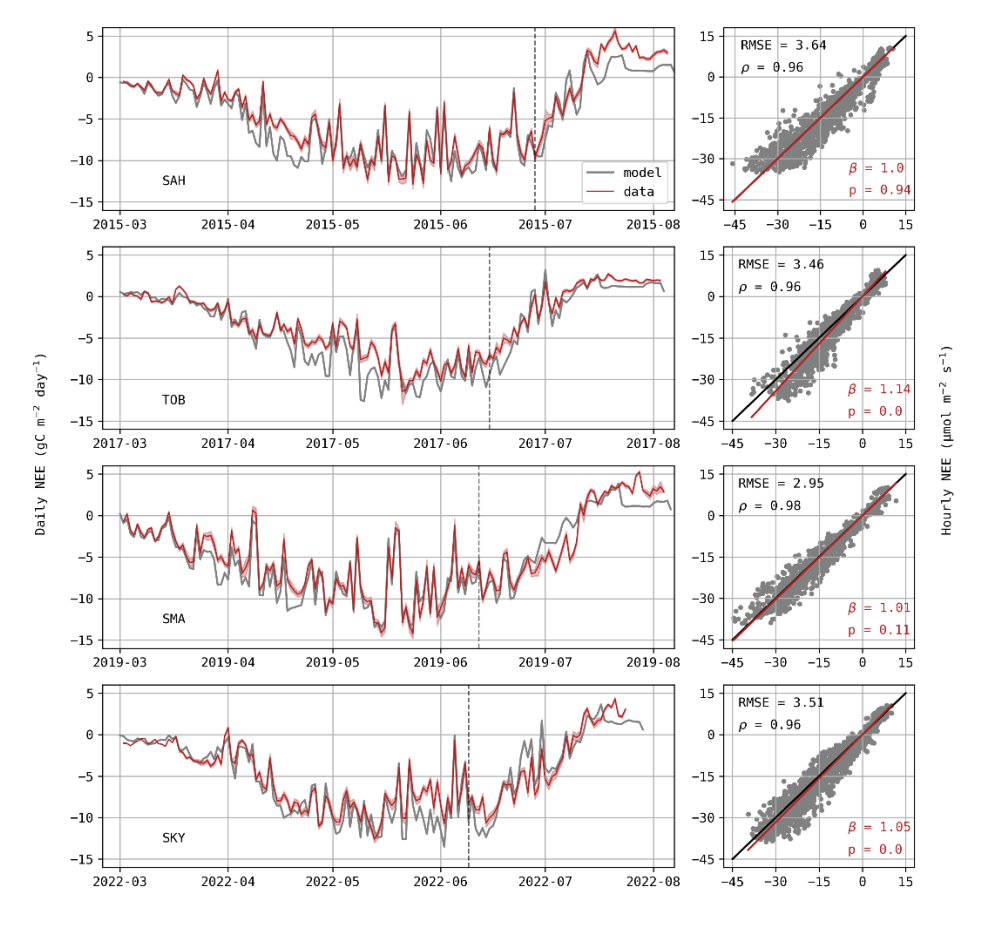


Figure 3: Daily NEE (gC m⁻² day⁻¹) for each growing season (left) with shaded area in red representing standard deviations of observations. Hourly predictions against observed values of NEE (μ mol m⁻² s⁻¹; right) where observed values are displayed on the x-axis. The p-value indicates if the regression slope β (red) is significantly different from the 1:1 line (black) and ρ is the Pearson correlation coefficient.



220



As expected from the rRMSE values observed in Fig. 1, LE fluxes are not well captured by the model. Observed daily fluxes exhibit greater variations, frequently reaching high values or dropping below 50 Wm⁻² while simulated values remain relatively stable (Fig. 4). This is also illustrated in the scatter plots, where hourly observed data easily reach 600 Wm⁻², but simulated fluxes never exceed 500 Wm⁻², resulting in a poor linear agreement between observed and simulated fluxes as indicated by the low Pearson correlation coefficients ρ (Fig. 4). This disagreement is particularly visible in April 2019 (SMA season), with an observed daily average around 180 Wm⁻² in comparison with a prediction of only ~100 Wm⁻². During this period, simulated evapotranspiration equals potential evapotranspiration, suggesting that the plant was not water-limited and that the underestimation stems from deficiencies in energy partitioning rather than water availability.

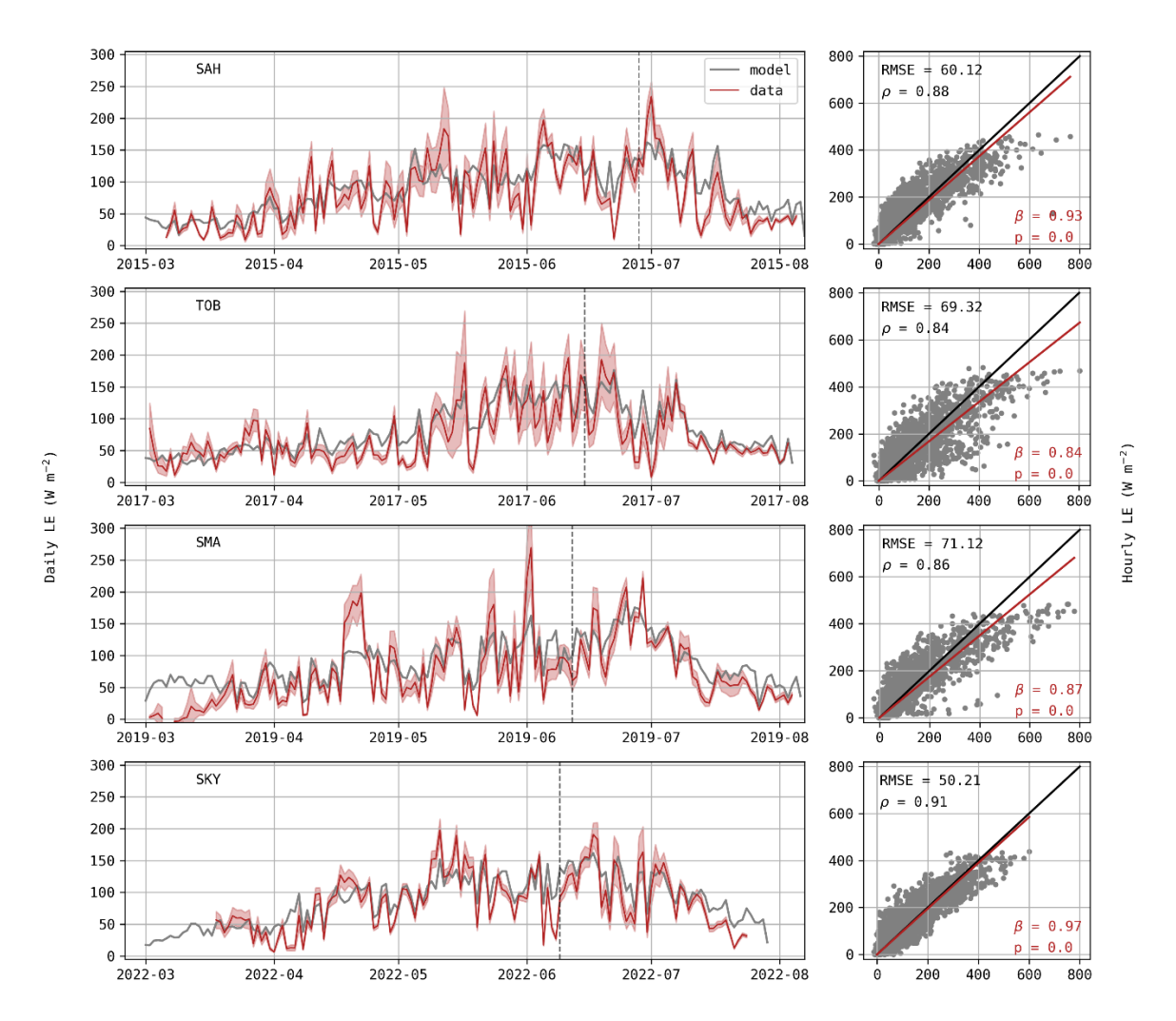


Figure 4: Daily average of LE (W m⁻²) for each growing season (left) with shaded area in red representing standard deviations of observations. Hourly predictions against observed values of LE (right) where observed values are displayed on the x-axis. The p-value indicates if the regression slope β (red) is significantly different from the 1:1 line (black) and ρ is the Pearson correlation coefficient.



230

235



Even though there was no apparent soil water deficit, this period (April 18 – April 22) was still characterised by elevated temperatures and higher vapour pressure deficit (VPD) compared to preceding days. It does not meet the formal Belgian definition of a heatwave, but the daily mean temperatures were more than 5° C above the 1981-2010 averages. During this 5-day period, the observed stomatal conductance g_s reached extremely high values (Fig. 5a), associated with an important increase in LE fluxes (Fig. 5c) while the magnitude of the carbon uptake (GPP) was not affected (Fig. 5b). These observations reveal a decrease in water use efficiency during this period, indicating that transpiration was intensified with no corresponding increase in carbon assimilation. This trend was not captured by the model, as simulated g_s remained lower than 0.03 m s⁻¹ (Fig. 5a). The slight increase in predicted g_s during the 5 days can be explained by the minor increase in carbon uptake (Fig. 5b).

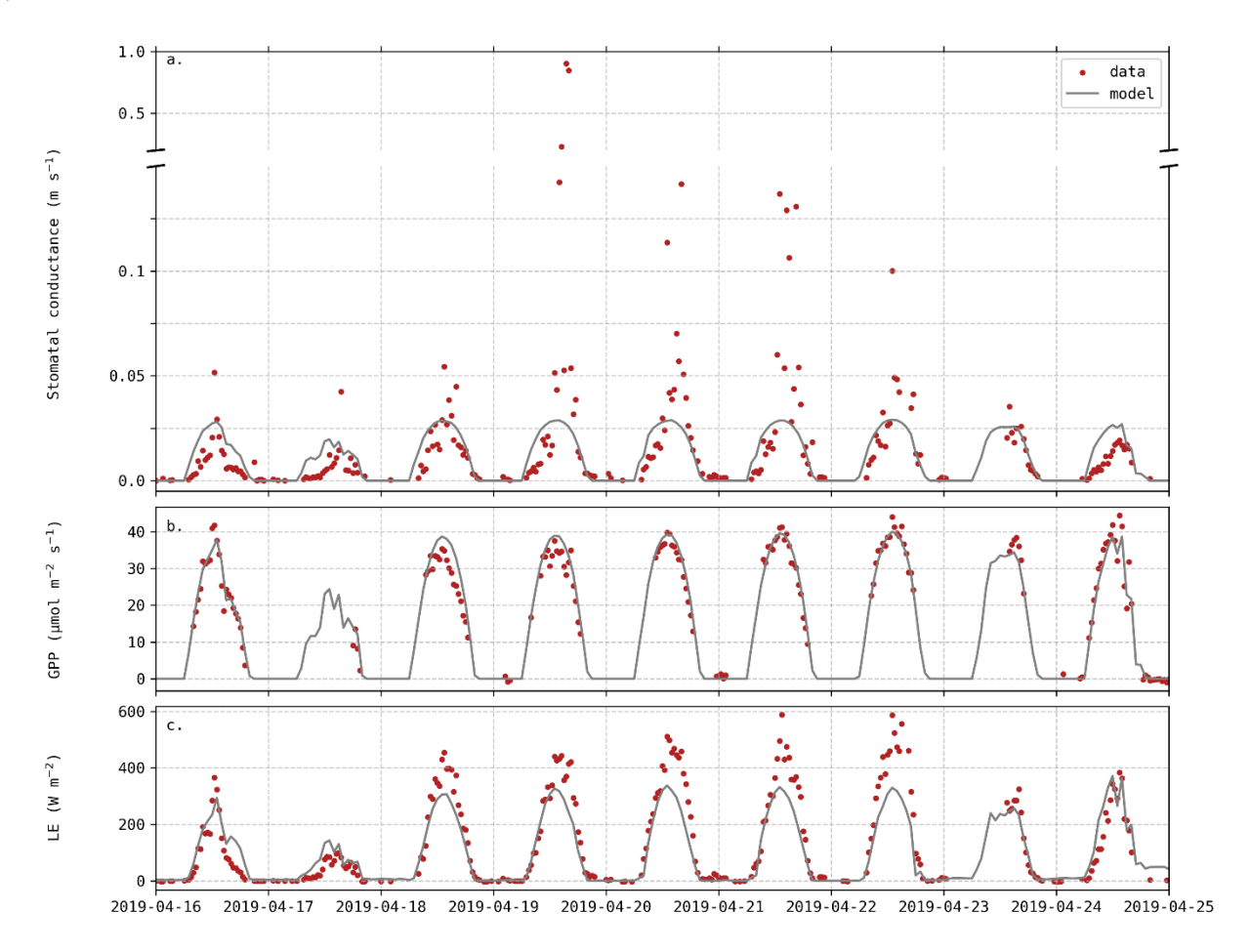


Figure 5: Evolution of predicted and observed (a) stomatal conductance g_s , (b) Gross Primary Productivity (GPP) and (c) LE fluxes.

Observed g_s was deduced from Penman–Monteith equation, measured fluxes and weather data (Appendix C). The axis break indicates different scales but does not imply omitted observations.





3.4 Validation

245

When using the most-balanced parameter set on VAL growing season, NEE is well reproduced by the model with an EF greater than 0.8, a rRMSE around 40% and a NME close to 0 for both time scales (Table 1a). Although rRMSE and EF also present acceptable results for DM, it is worth noting that there is an overall underestimation of this variable (NME = -0.222).

Table 3: Evaluation criteria for the 2010-2011 growing season using (a) the most-balanced parameter set (red point) and (b) the parameter set minimising F_{LE} . RMSE are expressed in W m^{-2} for LE, in $\mu mol\ m^{-2}s^{-1}$ for hourly NEE, in $gC\ m^{-2}d^{-1}$ for daily NEE and in $t\ ha^{-1}$ for DM. Other criteria have no units.

	a. Most-balanced parameter set			b. LE-oriented parameter set					
Variable	Resolution	RMSE	rRMSE	NME	EF	RMSE	rRMSE	NME	EF
LE	Hourly	99.6	0.706	0.203	0.420	97.3	0.689	0.177	0.447
	Daily	52.3	0.901	0.551	-0.353	48.6	0.831	0.503	-0.172
NEE	Hourly	4.21	0.442	-0.00104	0.899	4.89	0.514	-0.0925	0.865
	Daily	1.78	0.383	0.0463	0.870	2.24	0.484	-0.0821	0.795
DM	Daily	2.09	0.387	-0.222	0.807	2.38	0.441	-0.271	0.749

On the other hand, there is no good agreement between observed and predicted LE, especially when considering daily time scale, as shown by the four indicators. Even when using the parameter set that minimises F_{LE} (Fig. 1a), LE remains poorly captured by the model (Table 1b). As expected from the Pareto front, this slight improvement in LE predictions is accompanied with a degradation of NEE and DM predictions.





4 Discussion

260

265

270

285

4.1 Pareto-based calibration

Considering all objectives, the chosen parameter set (red point in Fig. 1) show satisfying fitting results, with a total RMSE of 0.948 t ha^{-1} , 3.44 $\mu mol\ m^{-2}s^{-1}$ and 62.7 W m^{-2} for DM, NEE and LE respectively. As a comparison with other models, calibrated RMSE values for total biomass are typically between 0.5 and 1.5 t ha^{-1} (Zhang et al., 2020; Dumont et al., 2014; Casanova and Judge, 2008). Regarding NEE, reported RMSE values for daily fluxes range from 1.3 to 1.9 gC m^{-2} d^{-1} (Revill et al., 2019; Senapati et al., 2018; Lehuger et al., 2010). In the present study, the RMSE computed from hourly NEE (3.44 $\mu mol\ m^{-2}\ s^{-1}$) corresponds to a RMSE of 1.49 gC m^{-2} d^{-1} when using daily fluxes, which falls in the mentioned range. Casanova and Judge (2008) reported a RMSE of 62.45 W m^{-2} for hourly LE fluxes and other studies presented values ranging from 24.65 to 48.5 W m^{-2} for daily fluxes (Wang et al., 2024; Liu F. et al., 2020; Dutta et al., 2016), while we found 30.74 W m^{-2} using daily averages.

In addition to provide reliable solutions, Pareto-based multi-objective calibration also offers insights into internal model limitations (Kollat et al., 2012). As related by Schoups et al. (2005), the shape of the Pareto front is an indicator of model structural error. Angular fronts (e.g., NEE–LE front) suggest that different objectives can be simultaneously optimised whereas significant trade-offs (curved or linear fronts) may indicate a wrong parameterisation of the model (Wöhling et al., 2013; Efstratiadis and Koutsoyiannis, 2010). The following sections focus on the NEE–DM and NEE–LE trade-offs and discuss whether the disagreements between observations and model predictions come from uncertainty due to measurement errors or deeper structural issues.

4.2 Where does the carbon go?

As shown by the major trade-off in Fig. 1b, adjusting model parameters to fit NEE fluxes inevitably compromises the simulation of organ DM. The analysis in Sect. 3.2 and 3.3 reveals that this would specifically result in an underestimation of biomass. Indeed, DM during vegetative stage is well reproduced when simulated NEE is overly negative, and *SOrg* DM is underestimated when NEE predictions show less bias (Fig. 2 and 3). This was also observed in the validation results, with a consistent underestimation of DM while NEE showed neither over- nor underestimation. Several factors may contribute to this mismatch:

Underestimation of heterotrophic respiration. If so, as respiration is regarded as positive and photosynthesis as negative with the micro-meteorological sign convention, NEE predictions would be too negative (as observed). Improving heterotrophic respiration would affect NEE predictions but its influence on DM would be limited, which could weaken the trade-off between these variables. At this study site, Suleau et al. (2011) partitioned soil respiration into its heterotrophic and autotrophic components using soil chambers, from which they derived temperature functions. When comparing their fitted regression to simulated heterotrophic respiration, Daisy appears to underestimate both temperature sensitivity and baseline respiration rate for three growing seasons (Fig. D1), supporting this first assumption. It should be noted, however, that this regression depends



290

295

300

305

310

315



solely on temperature, ignoring the seasonal variation in residue and fertilisation inputs that also affect soil respiration dynamics. Furthermore, heterotrophic respiration is most likely to be underestimated as, during the bare soil period before sowing, NEE (which only consists of soil respiration at that time) is mostly underestimated (Table D2).

Incorrect dry matter partitioning. Leaves are the major contributor to photosynthesis while stem reserves fuel grain filling during the reproductive stage. Thus, dry matter partitioning is critical for simulating accurately DM but may influence NEE predictions differently. For instance, if too much assimilated carbon is allocated to the roots at the expense of the stem, the model would underestimate stem and *SOrg* DM without altering leaf photosynthesis. For this study, the partitioning schemes were derived from SKY season since root measurements were only made during that season, as well as early distinction between leaf and stem. Consequently, partitioning coefficients might be inadequate for other growing seasons and partly contribute to this trade-off.

Wrong structural assumptions. Modelling real-world system comes with simplifications. For instance, in this study, Specific Leaf Area (SLA) was assumed to be constant throughout the season, although it's proved to vary with leaf age and other environmental factors (Liu Zhaogang et al., 2023; Zhou et al., 2020). Since SLA governs the conversion between leaf DM and leaf area index, using a constant value may lead to significant bias in photosynthesis and canopy development.

Uncertainties and errors in NEE observations. Eddy covariance (EC) data are affected by multiple factors, including instrumental noise, frequency losses and turbulence conditions (Aubinet et al., 2012). To account for these, EC data are thoroughly filtered, and their uncertainty is quantified combining random errors and uncertainty related to the friction velocity, an indicator of turbulence strength (Pastorello et al., 2020). However, an additional source of errors has been discussed in relation to the energy balance closure problem (Gao et al., 2019). EC systems show a systematic underestimation of energy fluxes (sensible and latent heat) ranging from 15 to 20% which is generally attributed to sub-mesoscale organised structures, generated in the daytime convective layer and enhanced by underlying surface heterogeneities (Mauder et al., 2020; Aubinet et al., 2012). While a standard correction method exists for energy fluxes (Pastorello et al., 2020), its application to CO₂ fluxes remains under active research (Mauder et al., 2024). Some studies suggest that CO₂ fluxes may also be underestimated (Gao et al., 2019; Mauder et al., 2010), though Liu H. et al. (2024) found that the bias rather depends on soil water conditions. At BE-Lon, this potential underestimation of CO₂ fluxes is supported by the crop carbon budget previously estimated (Buysse et al., 2017). When combining NEE and field (harvest, residues and inputs) measurements, they found that the study site continuously loses an unexpectedly large amount of carbon, depleting the soil much faster than recently observed (Dumont et al., 2025). This highlights that, beyond random error estimates, systematic biases in NEE measurements may propagate into model calibration and interpretation. As Beven (2019) emphasizes, observational datasets should not be treated as absolute truth, and acknowledging these uncertainties is important when designing calibration frameworks or interpreting model evaluations.



330

335



320 4.3 Structural limitations in simulating LE

When there is no evaporation from free water surfaces, the surface water balance in Daisy can be summarised as:

- 1. computation of potential evapotranspiration (PET) using the FAO56 equation
- 2. partitioning of PET between potential soil evaporation and plant transpiration according to canopy cover
- 3. computation of actual soil evaporation, depending on soil water availability
- 4. numerical resolution of Farquhar–Leuning models simultaneously with the SVAT module (surface energy balance) to obtain actual transpiration, surface temperatures and carbon assimilation.

Model limitations may arise from this workflow in two ways. First, the evapotranspiration (ET) is constrained by FAO56 PET which assumes a fixed stomatal conductance (Allen et al., 2006). Although it is widely used in crop modelling, this simplification can reduce the accuracy of ET estimations (Liu Ziwei et al., 2023; Ghiat et al., 2021). By considering a constant g_s for PET, simulated ET can be severely limited when stomata are actually wide open. Conversely, when stomata are closed, PET is overestimated and can therefore lead to higher soil evaporation than observed. This may partly explain the lack of temporal variation observed in Fig. 4 and the high values of rRMSE (Fig. 1c).

Second, soil evaporation (E_{soil}) is computed outside the iteration loop that couples the SVAT module with the Farquhar–Leuning models. It is constrained either by soil water availability or by the potential evaporative demand, depending on which is limiting. By contrast, fully coupled models such as CLM calculate resistance-based E_{soil} simultaneously with transpiration and sensible heat fluxes (Swenson and Lawrence, 2014). This ensures that E_{soil} is driven by microclimate conditions (e.g. canopy air vapour pressure) and reinforces the mechanistic coupling between the surface energy and water balances. However, the appropriate formulation of resistance-based E_{soil} remains an active research area, as recent studies continue to refine its parameterisation and physical basis (Schulz and Vogel, 2020; Lehmann et al., 2018).

Beside these workflow aspects, the relatively narrow Pareto shape (Fig. 1c) suggests the presence of equifinality, that is when multiple parameter sets produce equally good results (Her and Seong, 2018). This likely reflects compensatory interactions between soil evaporation and plant transpiration. Since PET is partitioned by canopy cover, parameter changes that alter canopy development can redistribute PET between the two components while leaving total PET unaffected. Under non-stressed water conditions, the ecosystem would meet this evaporative demand, and total ET (i.e. LE outputs) would remain unchanged as well. This masking effect underscores the well-known challenge of ET partitioning in ecosystem modelling, further complicated as eddy covariance systems do not distinguish between soil evaporation and transpiration (Berg and Sheffield, 2019; Stoy et al., 2019; Scott and Biederman, 2017). Recent methods such as flux mapping have been developed to better understand model internal fluxes leading to equifinality (Khatami et al., 2019).

As depicted by Fig. 5, discrepancies in LE predictions were especially evident under elevated temperatures and high VPD.

While these may partly stem from limitations mentioned above, they also point to deeper issues in the coupling between Farquhar and Leuning models and particularly in how it responds to atmospheric drivers.



355

365

375

380



4.4 Coupling of carbon and water exchanges

Stomatal behaviour plays a central role in plant regulation of water loss and carbon uptake, and has therefore been extensively studied (Damour et al., 2010). While it is well established that mild edaphic drought induces a decrease in carbon assimilation by reducing the stomatal aperture (Beauclaire et al., 2024), plant responses to heatwaves and high atmospheric demand are less evident. Most studies report reduced g_s under high VPD (Grossiord et al., 2020; Bourbia and Brodribb, 2024), aligning with the theoretical predictions of stomatal models (Sabot et al., 2022). On the other hand, high temperatures seem to trigger stomatal opening to promote transpiration cooling (Urban et al., 2017), but reported results vary greatly among species (Moore et al., 2021).

Under the combined effect of high temperature and VPD, Marchin et al. (2022) observed a significant increase in g_s for two well-watered species, interpreting this as a strategy to prevent leaf overheating via enhanced LE loss without any increase in carbon assimilation. They later confirmed that this behaviour, referred to as stomatal decoupling, is not restricted to well-watered species (Marchin et al., 2023).

In our results, wheat SMA variety appeared to exhibit a similar cooling strategy in April 2019 (Fig. 5), with increased transpiration contributing to heat dissipation as soil water was easily accessible. Plants likely opened their stomata, promoting water loss, while carbon assimilation did not increase accordingly. Inside the leaf, CO₂ diffuses through air spaces and membranes to reach the sites of carboxylation inside chloroplasts, whereas H₂O moves from the xylem network to the stomata (Flexas et al., 2012; Sack and Holbrook, 2006). Thus, these different pathways can be affected independently, where carbon assimilation can be restricted by non-stomatal factors, often dominated by mesophyll conductance (Flexas et al., 2012).

Based on stomatal coupling, Daisy does not fully capture these dynamic responses. According to Leuning model (Eq. 1), the increase in VPD reduces the predicted slope between carbon assimilation and g_s . Consequently, the model tends to underestimate g_s and LE fluxes and overestimate sensible heat, leading to a misrepresentation of energy partitioning under such conditions.

This decoupling behaviour was particularly visible in April 19, as the heatwave lasted several days, but also appeared during shorter warm periods for other growing seasons, suggesting that it represents a recurrent plant strategy. Future work should investigate and incorporate in crop models (i) the physiological mechanisms driving increased g_s under such conditions and (ii) the non-stomatal limitations affecting carbon assimilation.

5 Conclusion

In this study, we employed a Pareto-based multi-objective calibration approach to optimise the Daisy soil-plant-atmosphere model, focusing on three key objectives (DM, NEE and LE). The SMPSO algorithm successfully identified parameter sets that balanced these objectives within realistic bounds. Furthermore, this methodology also offered valuable insights into model behaviour and inherent limitations, as particular trade-offs between the objectives were revealed. Notably, the strong compromise between DM and NEE suggests possible wrong parameterisations of the model and biases in observational EC



390

395



data. Similarly, the LE-NEE trade-off indicates issues of equifinality which underlines the challenging partitioning of evapotranspiration. The inaccuracy of LE predictions was also discussed, underscoring the oversimplification of FAO56 Penman-Monteith method.

Additionally, the model struggled to reproduce observed increases in transpiration during heatwave conditions, highlighting deficiencies in simulating stomatal responses and in the coupling between carbon and water fluxes. These limitations are particularly relevant given the increasing frequency and intensity of heatwaves under climate change, which can significantly impact ecosystem dynamics. The influence of heatwaves and underlying mechanisms of stomatal decoupling need to be further investigated in order to improve the simulation of energy fluxes.

Overall, this work illustrates how multi-objective calibration can go beyond parameter estimation to critically assess model assumptions and guide future improvements. Addressing the structural limitations identified here – particularly in ET partitioning and (non-)stomatal regulation – could strengthen the ability of Daisy and similar crop models to capture ecosystem responses under changing climate conditions.





Appendices

400

Appendix A: Daisy modification

Diffuse fraction. The diffuse fraction of global radiation f_d was estimated using the optical air mass and assuming a cloudless sky (Appendix 1 of de Pury and Farquhar, 1997). A second modelling option for estimating f_d , adapted for cloudy skies, was implemented. Based on Ridley et al. (2010), f_d depends on the hourly and daily clearness index (resp. k_t and K_t), the apparent solar time (AST) and the solar angle α :

$$f_d = \frac{1}{1 + e^{\beta_0 + \beta_1 k_t + \beta_2 AST + \beta_3 \alpha + \beta_4 K_t}},\tag{A1}$$

As both diffuse and global radiation are measured at BE-Lon, the five β parameters have been estimated with the Nelder–Mead method, considering the RMSE metric as objective function. This method has been applied to 10 years of measurements (2014–2023), covering the entire duration of the case study. The resulting parameters (β_0 , β_1 , β_2 , β_3 , β_4) are respectively equal to -4.8094, 5.4735, 0.020702, 0.099970 and 1.3944 (RMSE for $f_d = 0.164$).

Maintenance respiration. Respiration required to maintain existing biomass is defined as maintenance respiration. In Daisy, the maintenance respiration of an organ R_m^{org} is proportional to its dry weight W^{org} :

$$R_m^{org} = r_m^{org} \cdot f(T) \cdot W^{org} , \qquad (A2)$$

- where r_m^{org} is the maintenance respiration coefficient of the organ and f(T) is a temperature function. In addition to temperature dependence, it was demonstrated that mature or senescing tissues required lower maintenance than younger tissues (Boote et al., 2013). Maintenance respiration declines near the end of the growing season due to a significant fraction of dead cells and metabolically inactive long-term storage (Amthor, 2025). To account for this, a second dependency f(DS) was added into Eq. A2 and is a user-defined function of development stage.
- *Remobilisation*. After anthesis, carbon reserves stored in the stem can be mobilised to support grain filling. The remobilisation equations in Daisy were modified to account for both remobilisation efficiency and the temporal dynamics of the remobilisation rate. This rate peaks around 20 days after anthesis before declining, resulting in a sigmoid-shaped depletion of stem reserves (Liu Y. et al., 2020; Ehdaie et al., 2008).





420 Appendix B: Most balanced parameter set

Table B1: Most balanced parameter set among non-dominated solutions (red point in Fig. 1).

Parameter	SAH	TOB	SMA	SKY	Units
fPSII	0.3668	0.3291	0.3645	0.4009	-
Xn	7.929e-4	7.550e-4	1.076e-3	6.835e-4	mol mol ⁻¹ s ⁻¹
Do	3354	2820	1596	2820	Pa
${g}_1$	10.54	14.87	14.79	16.79	-
${g}_0$	0.01335	9.079e-3	0.01658	0.01324	$mol m^{-2} s^{-1}$
δ	0.3635	0.1940	0.4816	0.8232	-
SpLAI	0.01598	0.02103	0.02143	0.01522	$m^2 g^{-1}$
ShldResC	49.45	47.60	41.98	42.54	%
NNI_{crit}	1.373	1.470	1.444	1.346	-
SOrgPhotEff	0.7227	0.2565	0.1808	0.6703	-
StemPhotEff	0.09723	0.7164	0.2039	0.7606	-
PenPar2		4.8	322		°C
σ_{NIR}		-			
$arepsilon_{leaf}$		-			
k_{net}		-			
A_{brunt}		-			
B_{brunt}		hPa ^{-1/2}			
Ke		=			
Kc		=			
$K_{sat,1}$		cm h ⁻¹			
$K_{aquitard}$		cm h ⁻¹			
$Z_{aquitard}$		1.9	974		m





Appendix C: Determination of stomatal conductance

According to Penman-Monteith equation, the latent heat flux (LE) can be expressed as follows:

$$LE = \frac{\Delta (R_n - G) + \frac{\rho_a c_p VPD}{r_a}}{\Delta + \gamma \left(1 + \frac{r_s}{r_a}\right)},$$
(C1)

where R_n is the net irradiance $(W \ m^{-2})$, G is the ground heat flux $(W \ m^{-2})$, VPD is the Vapour Pressure Deficit (Pa), ρ_a is the dry air density (equal to 1.22 $kg \ m^{-3}$), c_p is the specific heat capacity of air (equal to 1013 $J \ kg^{-1} \ {}^{\circ}C^{-1}$) and r_s is the stomatal resistance $(r_s = g_s^{-1})$. The slope of the saturation vapour pressure with temperature Δ can be estimated based on vapour pressure at saturation $e^*(T_{air})$:

430
$$\Delta = \frac{4098 \, e^* (T_{air})}{(T_{air} + 237.3)^2},$$
 (C2)

The psychometric constant γ is a function of atmospheric pressure P:

$$\gamma = \frac{c_p P}{0.622 \cdot 2.45 \cdot 10^6},\tag{C3}$$

And finally, the atmospheric resistance r_a is composed of the aerodynamic and boundary layer resistances:

$$r_a = \left(\frac{u}{u}\right)^2 + 6.2u_*^{-0.67},\tag{C4}$$

As LE, G, R_n , VPD, the air temperature T_{air} , P, the wind velocity u, the friction velocity u_* are directly measured or at least computed within the ONEFlux pipeline (Pastorello et al., 2020), the stomatal resistance can be determined by combining equations C1–C4.





Appendix D: Heterotrophic respiration

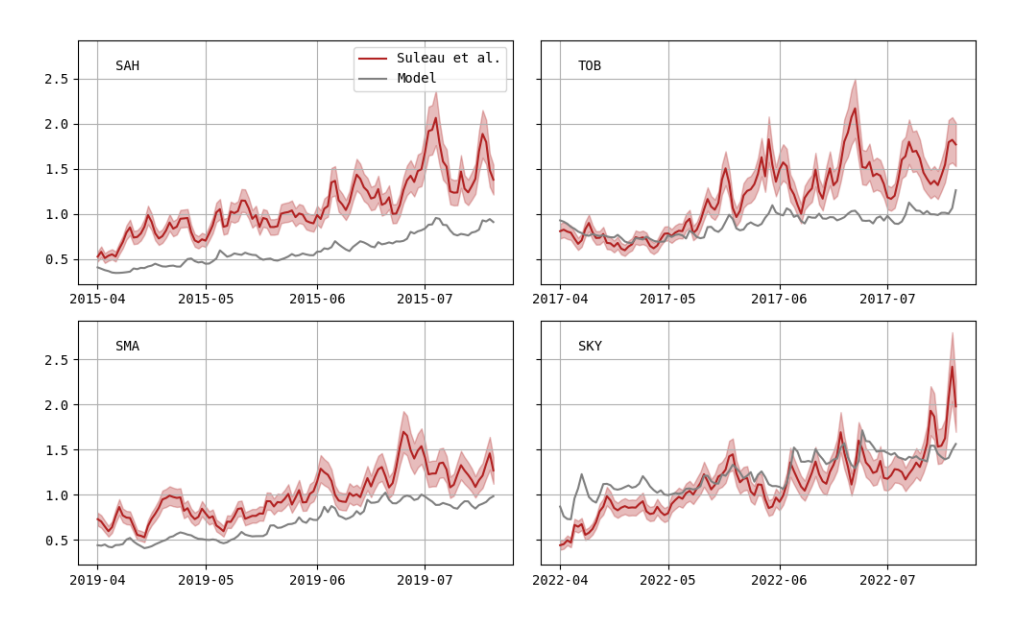


Figure D1: Daily evolution of heterotrophic respiration (gC m⁻² day⁻¹) – model predictions (grey) and estimations based on the temperature function fitted by Suleau et al. (2011; red).

Table D2: Evaluation criteria regarding daily NEE during the bare soil period before sowing. RMSE and ME are expressed in $gC m^{-2} d^{-1}$ and other criteria have no units. VAL growing season was simulated with the most-balanced parameter set (SAH cultivar).

Season	RMSE	rRMSE	ME	NME
SAH	0.320	0.308	0.0144	0.0139
TOB	0.736	0.422	-0.0493	-0.0282
SMA	0.228	0.190	-0.0484	-0.0403
SKY	0.622	0.289	-0.490	-0.228
VAL	0.484	0.376	-0.237	-0.184

https://doi.org/10.5194/egusphere-2025-4987 Preprint. Discussion started: 27 November 2025

© Author(s) 2025. CC BY 4.0 License.



450



Code and data availability

Daisy is an open-source model developed by the Agrohydrology group at the University of Copenhagen, Denmark, and is available on GitHub (https://github.com/daisy-model/daisy). All Python scripts, as well as input and setup files used for running Daisy, are also accessible on GitHub (Delhez, 2025). Flux and meteorological data for BE-Lon can directly be downloaded on the ICOS Data Portal for the 2004–2020 period (Heinesch et al., 2022). More recent (2021–2024) data using the same workflow have been submitted to the Ecosystem Thematic Centre (ETC) for official publishing, but in the meantime can be accessed upon request.

Author contributions

EL, BL and LD designed the main conceptual ideas, EL and LD implemented the calibration method, LD made amendments to the model code, QB, BL and LD analysed the data, and LD prepared the manuscript with contributions from all co-authors.

Competing interests

The authors declare that they have no conflict of interest.

Acknowledgements

We would like to thank Ariane Faurès and Bernard Heinesch (and all ICOS Wallonia) for providing data and assistance, as well as the Daisy team for the useful discussions. This research is supported by the Federation Wallonie Bruxelles (FWB).





References

- Abrahamsen, P. and Hansen, S.: Daisy: an open soil-crop-atmosphere system model, Environmental Modelling & Software, 15, 313–330, https://doi.org/10.1016/S1364-8152(00)00003-7, 2000.
- Allen, R. G., Pereira, L. S., Raes, D., and Smith, M.: Crop evapotranspiration: Guidelines for computing crop water requirements, edited by: Food and Agriculture Organization of the United Nations, Food and Agriculture Organization of the United Nations, Rome, 300 pp., 1998.
 - Allen, R. G., Pruitt, W. O., Wright, J. L., Howell, T. A., Ventura, F., Snyder, R., Itenfisu, D., Steduto, P., Berengena, J., Yrisarry, J. B., Smith, M., Pereira, L. S., Raes, D., Perrier, A., Alves, I., Walter, I., and Elliott, R.: A recommendation on
- standardized surface resistance for hourly calculation of reference ETo by the FAO56 Penman-Monteith method, Agricultural Water Management, 81, 1–22, https://doi.org/10.1016/j.agwat.2005.03.007, 2006.
 - Amthor, J. S.: After photosynthesis, what then: Importance of respiration to crop growth and yield, Field Crops Research, 321, 109638, https://doi.org/10.1016/j.fcr.2024.109638, 2025.
 - Asseng, S., Martre, P., Maiorano, A., Rötter, R. P., O'Leary, G. J., Fitzgerald, G. J., Girousse, C., Motzo, R., Giunta, F., Babar,
- M. A., Reynolds, M. P., Kheir, A. M. S., Thorburn, P. J., Waha, K., Ruane, A. C., Aggarwal, P. K., Ahmed, M., Balkovič, J., Basso, B., Biernath, C., Bindi, M., Cammarano, D., Challinor, A. J., De Sanctis, G., Dumont, B., Eyshi Rezaei, E., Fereres, E., Ferrise, R., Garcia-Vila, M., Gayler, S., Gao, Y., Horan, H., Hoogenboom, G., Izaurralde, R. C., Jabloun, M., Jones, C. D., Kassie, B. T., Kersebaum, K.-C., Klein, C., Koehler, A., Liu, B., Minoli, S., Montesino San Martin, M., Müller, C., Naresh Kumar, S., Nendel, C., Olesen, J. E., Palosuo, T., Porter, J. R., Priesack, E., Ripoche, D., Semenov, M. A., Stöckle, C.,
- Stratonovitch, P., Streck, T., Supit, I., Tao, F., Van Der Velde, M., Wallach, D., Wang, E., Webber, H., Wolf, J., Xiao, L., Zhang, Z., Zhao, Z., Zhu, Y., and Ewert, F.: Climate change impact and adaptation for wheat protein, Global Change Biology, 25, 155–173, https://doi.org/10.1111/gcb.14481, 2019.
 - Aubinet, M., Vesala, T., and Papale, D. (Eds.): Eddy Covariance: A Practical Guide to Measurement and Data Analysis, Springer Netherlands, Dordrecht, https://doi.org/10.1007/978-94-007-2351-1, 2012.
- Beauclaire, Q., Vanden Brande, F., and Longdoz, B.: Key role played by mesophyll conductance in limiting carbon assimilation and transpiration of potato under soil water stress, Front. Plant Sci., 15, 1500624, https://doi.org/10.3389/fpls.2024.1500624, 2024.
 - Benítez-Hidalgo, A., Nebro, A. J., García-Nieto, J., Oregi, I., and Del Ser, J.: jMetalPy: A Python framework for multi-objective optimization with metaheuristics, Swarm and Evolutionary Computation, 51, 100598, https://doi.org/10.1016/j.swevo.2019.100598, 2019.
 - Berg, A. and Sheffield, J.: Evapotranspiration Partitioning in CMIP5 Models: Uncertainties and Future Projections, Journal of Climate, 32, 2653–2671, https://doi.org/10.1175/JCLI-D-18-0583.1, 2019.
 - Beven, K.: Towards a methodology for testing models as hypotheses in the inexact sciences, Proc. R. Soc. A., 475, 20180862, https://doi.org/10.1098/rspa.2018.0862, 2019.



510



- Boote, K. J., Jones, J. W., White, J. W., Asseng, S., and Lizaso, J. I.: Putting mechanisms into crop production models, Plant Cell & Environment, 36, 1658–1672, https://doi.org/10.1111/pce.12119, 2013.
 - Bourbia, I. and Brodribb, T. J.: Stomatal response to VPD is not triggered by changes in soil–leaf hydraulic conductance in *Arabidopsis* or *Callitris*, New Phytologist, 242, 444–452, https://doi.org/10.1111/nph.19607, 2024.
- Buysse, P., Bodson, B., Debacq, A., De Ligne, A., Heinesch, B., Manise, T., Moureaux, C., and Aubinet, M.: Carbon budget measurement over 12 years at a crop production site in the silty-loam region in Belgium, Agricultural and Forest Meteorology, 246, 241–255, https://doi.org/10.1016/j.agrformet.2017.07.004, 2017.
 - Cameron, D., Hartig, F., Minnuno, F., Oberpriller, J., Reineking, B., Van Oijen, M., and Dietze, M.: Issues in calibrating models with multiple unbalanced constraints: the significance of systematic model and data errors, Methods Ecol Evol, 13, 2757–2770, https://doi.org/10.1111/2041-210X.14002, 2022.
- Casanova, J. J. and Judge, J.: Estimation of energy and moisture fluxes for dynamic vegetation using coupled SVAT and cropgrowth models, Water Resources Research, 44, 2007WR006503, https://doi.org/10.1029/2007WR006503, 2008.
 - Damour, G., Simonneau, T., Cochard, H., and Urban, L.: An overview of models of stomatal conductance at the leaf level: Models of stomatal conductance, Plant, Cell & Environment, no-no, https://doi.org/10.1111/j.1365-3040.2010.02181.x, 2010. De Ligne, A., Heinesch, B., and Aubinet, M.: New Transfer Functions for Correcting Turbulent Water Vapour Fluxes,
 - Deb, K.: Multi-objective optimization using evolutionary algorithms, J. Wiley, Chichester New York Weinheim [etc.], 2001. Delhez, L.: LauraDelhez/Daisy_ParetoMOO: SMPSO-Daisy scripts and inputs, , https://doi.org/10.5281/ZENODO.16836123, 2025.

Boundary-Layer Meteorol, 137, 205–221, https://doi.org/10.1007/s10546-010-9525-9, 2010.

- Delhez, L., Dumont, B., and Longdoz, B.: Leveraging temporal variability in global sensitivity analysis of the Daisy soil-plant-atmosphere model, European Journal of Agronomy, 165, 127533, https://doi.org/10.1016/j.eja.2025.127533, 2025.
- De Noblet-Ducoudré, N., Gervois, S., Ciais, P., Viovy, N., Brisson, N., Seguin, B., and Perrier, A.: Coupling the Soil-Vegetation-Atmosphere-Transfer Scheme ORCHIDEE to the agronomy model STICS to study the influence of croplands on the European carbon and water budgets, Agronomie, 24, 397–407, https://doi.org/10.1051/agro:2004038, 2004.
- Dumont, B., Leemans, V., Mansouri, M., Bodson, B., Destain, J.-P., and Destain, M.-F.: Parameter identification of the STICS
- 520 crop model, using an accelerated formal MCMC approach, Environmental Modelling & Software, 52, 121–135, https://doi.org/10.1016/j.envsoft.2013.10.022, 2014.
 - Dumont, B., Heinesch, B., Bodson, B., Bogaerts, G., Chopin, H., De Ligne, A., Demoulin, L., Douxfils, B., Engelmann, T., Faurès, A., Longdoz, B., Manise, T., Orgun, A., Piret, A., and Thyrion, T.: ETC L2 ARCHIVE from Lonzee, 2017–2024, 2025.
- Dutta, B., Smith, W. N., Grant, B. B., Pattey, E., Desjardins, R. L., and Li, C.: Model development in DNDC for the prediction of evapotranspiration and water use in temperate field cropping systems, Environmental Modelling & Software, 80, 9–25, https://doi.org/10.1016/j.envsoft.2016.02.014, 2016.





- Efstratiadis, A. and Koutsoyiannis, D.: One decade of multi-objective calibration approaches in hydrological modelling: a review, Hydrological Sciences Journal, 55, 58–78, https://doi.org/10.1080/02626660903526292, 2010.
- Ehdaie, B., Alloush, G. A., and Waines, J. G.: Genotypic variation in linear rate of grain growth and contribution of stem reserves to grain yield in wheat, Field Crops Research, 106, 34–43, https://doi.org/10.1016/j.fcr.2007.10.012, 2008.
 - Farquhar, G. D., Von Caemmerer, S., and Berry, J. A.: Models of Photosynthesis, Plant Physiology, 125, 42–45, https://doi.org/10.1104/pp.125.1.42, 2001.
 - Flexas, J., Barbour, M. M., Brendel, O., Cabrera, H. M., Carriquí, M., Díaz-Espejo, A., Douthe, C., Dreyer, E., Ferrio, J. P.,
- Gago, J., Gallé, A., Galmés, J., Kodama, N., Medrano, H., Niinemets, Ü., Peguero-Pina, J. J., Pou, A., Ribas-Carbó, M., Tomás, M., Tosens, T., and Warren, C. R.: Mesophyll diffusion conductance to CO2: An unappreciated central player in photosynthesis, Plant Science, 193–194, 70–84, https://doi.org/10.1016/j.plantsci.2012.05.009, 2012.
 - Gao, Z., Liu, H., Missik, J. E. C., Yao, J., Huang, M., Chen, X., Arntzen, E., and Mcfarland, D. P.: Mechanistic links between underestimated CO₂ fluxes and non-closure of the surface energy balance in a semi-arid sagebrush ecosystem, Environ. Res.
- 540 Lett., 14, 044016, https://doi.org/10.1088/1748-9326/ab082d, 2019.
 - van Genuchten, M. Th.: A Closed-form Equation for Predicting the Hydraulic Conductivity of Unsaturated Soils, Soil Science Soc of Amer J, 44, 892–898, https://doi.org/10.2136/sssaj1980.03615995004400050002x, 1980.
 - Ghiat, I., Mackey, H. R., and Al-Ansari, T.: A Review of Evapotranspiration Measurement Models, Techniques and Methods for Open and Closed Agricultural Field Applications, Water, 13, 2523, https://doi.org/10.3390/w13182523, 2021.
- Grossiord, C., Buckley, T. N., Cernusak, L. A., Novick, K. A., Poulter, B., Siegwolf, R. T. W., Sperry, J. S., and McDowell, N. G.: Plant responses to rising vapor pressure deficit, New Phytologist, 226, 1550–1566, https://doi.org/10.1111/nph.16485, 2020.
 - Guerreiro, A. P., Fonseca, C. M., and Paquete, L.: The Hypervolume Indicator: Computational Problems and Algorithms, ACM Comput. Surv., 54, 1–42, https://doi.org/10.1145/3453474, 2021.
- Hansen, S., Jensen, H. E., Nielsen, N. E., and Svendsen, H.: Simulation of nitrogen dynamics and biomass production in winter wheat using the Danish simulation model DAISY, Fertilizer Research, 27, 245–259, https://doi.org/10.1007/BF01051131, 1991.
 - Hansen, S., Abrahamsen, P., Petersen, C. T., and Styczen, M.: Daisy: Model Use, Calibration, and Validation, Transactions of the ASABE, 55, 1317–1335, https://doi.org/10.13031/2013.42244, 2012.
- Harvey, N., Marshall, L., and Vervoort, R. W.: Verifying model performance using validation of Pareto solutions, Journal of Hydrology, 621, 129594, https://doi.org/10.1016/j.jhydrol.2023.129594, 2023.
 - Heinesch, B., De Ligne, A., Manise, T., and Longdoz, B.: Warm winter 2020 ecosystem eddy covariance flux product from Lonzee, https://doi.org/10.18160/46P3-WT1D, 2022.
- Her, Y. and Seong, C.: Responses of hydrological model equifinality, uncertainty, and performance to multi-objective parameter calibration, Journal of Hydroinformatics, 20, 864–885, https://doi.org/10.2166/hydro.2018.108, 2018.





- Holbak, M., Abrahamsen, P., Hansen, S., and Diamantopoulos, E.: A Physically Based Model for Preferential Water Flow and Solute Transport in Drained Agricultural Fields, Water Resources Research, 57, e2020WR027954, https://doi.org/10.1029/2020WR027954, 2021.
- Jahandideh-Tehrani, M., Bozorg-Haddad, O., and Loáiciga, H. A.: Application of particle swarm optimization to water management: an introduction and overview, Environ Monit Assess, 192, 281, https://doi.org/10.1007/s10661-020-8228-z, 2020.
 - Keenan, T., Sabate, S., and Gracia, C.: Soil water stress and coupled photosynthesis—conductance models: Bridging the gap between conflicting reports on the relative roles of stomatal, mesophyll conductance and biochemical limitations to photosynthesis, Agricultural and Forest Meteorology, 150, 443–453, https://doi.org/10.1016/j.agrformet.2010.01.008, 2010.
- Kennedy, J. and Eberhart, R.: Particle swarm optimization, in: Proceedings of ICNN'95 International Conference on Neural Networks, ICNN'95 International Conference on Neural Networks, Perth, WA, Australia, 1942–1948, https://doi.org/10.1109/ICNN.1995.488968, 1995.
- Khatami, S., Peel, M. C., Peterson, T. J., and Western, A. W.: Equifinality and Flux Mapping: A New Approach to Model Evaluation and Process Representation Under Uncertainty, Water Resources Research, 55, 8922–8941, https://doi.org/10.1029/2018WR023750, 2019.
 - Kollat, J. B., Reed, P. M., and Wagener, T.: When are multiobjective calibration trade-offs in hydrologic models meaningful?, Water Resources Research, 48, 2011WR011534, https://doi.org/10.1029/2011WR011534, 2012.
- Kucharik, C. J.: Evaluation of a Process-Based Agro-Ecosystem Model (Agro-IBIS) across the U.S. Corn Belt: Simulations of the Interannual Variability in Maize Yield, Earth Interact., 7, 1–33, https://doi.org/10.1175/1087-580 3562(2003)007<0001:EOAPAM>2.0.CO;2, 2003.
 - Lehmann, P., Merlin, O., Gentine, P., and Or, D.: Soil Texture Effects on Surface Resistance to Bare-Soil Evaporation, Geophysical Research Letters, 45, https://doi.org/10.1029/2018GL078803, 2018.
 - Lehuger, S., Gabrielle, B., Cellier, P., Loubet, B., Roche, R., Béziat, P., Ceschia, E., and Wattenbach, M.: Predicting the net carbon exchanges of crop rotations in Europe with an agro-ecosystem model, Agriculture, Ecosystems & Environment, 139, 384–395, https://doi.org/10.1016/j.agee.2010.06.011, 2010.
 - Leuning, R.: A critical appraisal of a combined stomatal-photosynthesis model for C3 plants, Plant Cell Environ, 18, 339–355, https://doi.org/10.1111/j.1365-3040.1995.tb00370.x, 1995.
- Liu, F., Ying, C., Dengpan, X., Huizi, B., Fulu, T., and Quansheng, G.: Modeling crop growth and land surface energy fluxes in wheat–maize double cropping system in the North China Plain, Theor Appl Climatol, 142, 959–970, https://doi.org/10.1007/s00704-020-03353-7, 2020.
 - Liu, F., Andersen, M. N., and Jensen, C. R.: Capability of the 'Ball-Berry' model for predicting stomatal conductance and water use efficiency of potato leaves under different irrigation regimes, Scientia Horticulturae, 122, 346–354, https://doi.org/10.1016/j.scienta.2009.05.026, 2009.





- Liu, H., Liu, C., Huang, J., Desai, A. R., Zhang, Q., Ghannam, K., and Katul, G. G.: Scalar Flux Profiles in the Unstable Atmospheric Surface Layer Under the Influence of Large Eddies: Implications for Eddy Covariance Flux Measurements and the Non-Closure Problem, Geophysical Research Letters, 51, e2023GL106649, https://doi.org/10.1029/2023GL106649, 2024. Liu, K., Wang, Y., Magney, T. S., and Frankenberg, C.: Non-steady-state stomatal conductance modeling and its implications: from leaf to ecosystem, Biogeosciences, 21, 1501–1516, https://doi.org/10.5194/bg-21-1501-2024, 2024.
- Liu, Y., Zhang, P., Li, M., Chang, L., Cheng, H., Chai, S., and Yang, D.: Dynamic responses of accumulation and remobilization of water soluble carbohydrates in wheat stem to drought stress, Plant Physiology and Biochemistry, 155, 262–270, https://doi.org/10.1016/j.plaphy.2020.07.024, 2020.
 - Liu, Ziwei., Wang, T., Li, C., Yang, W., and Yang, H.: A physically-based potential evapotranspiration model for global water availability projections, Journal of Hydrology, 622, 129767, https://doi.org/10.1016/j.jhydrol.2023.129767, 2023.
- Liu, Zhaogang., Zhao, M., Zhang, H., Ren, T., Liu, C., and He, N.: Divergent response and adaptation of specific leaf area to environmental change at different spatio-temporal scales jointly improve plant survival, Global Change Biology, 29, 1144–1159, https://doi.org/10.1111/gcb.16518, 2023.
 - Lokupitiya, E., Denning, S., Paustian, K., Baker, I., Schaefer, K., Verma, S., Meyers, T., Bernacchi, C. J., Suyker, A., and Fischer, M.: Incorporation of crop phenology in Simple Biosphere Model (SiBcrop) to improve land-atmosphere carbon exchanges from croplands, Biogeosciences, 6, 969–986, https://doi.org/10.5194/bg-6-969-2009, 2009.
- Manzoni, S., Vico, G., Katul, G., Fay, P. A., Polley, W., Palmroth, S., and Porporato, A.: Optimizing stomatal conductance for maximum carbon gain under water stress: a meta-analysis across plant functional types and climates: Optimal leaf gas exchange under water stress, Functional Ecology, 25, 456–467, https://doi.org/10.1111/j.1365-2435.2010.01822.x, 2011.
 Marchin, R. M., Backes, D., Ossola, A., Leishman, M. R., Tjoelker, M. G., and Ellsworth, D. S.: Extreme heat increases
- 615 https://doi.org/10.1111/gcb.15976, 2022.
 - Marchin, R. M., Medlyn, B. E., Tjoelker, M. G., and Ellsworth, D. S.: Decoupling between stomatal conductance and photosynthesis occurs under extreme heat in broadleaf tree species regardless of water access, Global Change Biology, 29, 6319–6335, https://doi.org/10.1111/gcb.16929, 2023.

stomatal conductance and drought-induced mortality risk in vulnerable plant species, Global Change Biology, 28, 1133–1146,

- Mauder, M., Desjardins, R. L., Pattey, E., and Worth, D.: An Attempt to Close the Daytime Surface Energy Balance Using Spatially-Averaged Flux Measurements, Boundary-Layer Meteorol, 136, 175–191, https://doi.org/10.1007/s10546-010-9497-9, 2010.
 - Mauder, M., Foken, T., and Cuxart, J.: Surface-Energy-Balance Closure over Land: A Review, Boundary-Layer Meteorol, 177, 395–426, https://doi.org/10.1007/s10546-020-00529-6, 2020.
- Mauder, M., Jung, M., Stoy, P., Nelson, J., and Wanner, L.: Energy balance closure at FLUXNET sites revisited, Agricultural and Forest Meteorology, 358, 110235, https://doi.org/10.1016/j.agrformet.2024.110235, 2024.
 - Meza, R., Jacquemin, G., Dumont, B., Bacchetta, R., Heens, B., Mahieu, O., Blanchard, R., Monfort, B., Chavalle, S., De Proft, M., Gofflot, S., Van Remoortel, V., Sinnaeve, G., and Bodson, B.: Variétés, in: Live Blanc "Céréales," 2018.





- Meza, R., Crevits, C., Eylenbosch, D., Mahieu, O., Bonnave, M., Blanchard, R., Van der Verren, B., Godin, B., Faux, A.-M., Legrand, J., and Heens, B.: Variétés en froment d'hiver, in: Livre Blanc "Céréales," 2023.
- Moges, E., Demissie, Y., Larsen, L., and Yassin, F.: Review: Sources of Hydrological Model Uncertainties and Advances in Their Analysis, Water, 13, 28, https://doi.org/10.3390/w13010028, 2020.
 Moore, C. E., Meacham-Hensold, K., Lemonnier, P., Slattery, R. A., Benjamin, C., Bernacchi, C. J., Lawson, T., and Cavanagh, A. P.: The effect of increasing temperature on crop photosynthesis: from enzymes to ecosystems. Journal of
 - Cavanagh, A. P.: The effect of increasing temperature on crop photosynthesis: from enzymes to ecosystems, Journal of Experimental Botany, 72, 2822–2844, https://doi.org/10.1093/jxb/erab090, 2021.
- Mualem, Y.: A new model for predicting the hydraulic conductivity of unsaturated porous media, Water Resources Research, 12, 513–522, https://doi.org/10.1029/WR012i003p00513, 1976.
 - Nebro, A. J., Durillo, J. J., Garcia-Nieto, J., Coello Coello, C. A., Luna, F., and Alba, E.: SMPSO: A new PSO-based metaheuristic for multi-objective optimization, in: 2009 IEEE Symposium on Computational Intelligence in Multi-Criteria Decision-Making(MCDM), 2009 IEEE Symposium on Computational Intelligence in Multi-Criteria Decision-Making
- (MCDM), Nashville, TN, USA, 66–73, https://doi.org/10.1109/MCDM.2009.4938830, 2009.
 Palosuo, T., Kersebaum, K. C., Angulo, C., Hlavinka, P., Moriondo, M., Olesen, J. E., Patil, R. H., Ruget, F., Rumbaur, C., Takáč, J., Trnka, M., Bindi, M., Çaldağ, B., Ewert, F., Ferrise, R., Mirschel, W., Şaylan, L., Šiška, B., and Rötter, R.: Simulation of winter wheat yield and its variability in different climates of Europe: A comparison of eight crop growth models,
 - European Journal of Agronomy, 35, 103–114, https://doi.org/10.1016/j.eja.2011.05.001, 2011.
- Pastorello, G., Trotta, C., Canfora, E., Chu, H., Christianson, D., Cheah, Y.-W., Poindexter, C., Chen, J., Elbashandy, A., Humphrey, M., Isaac, P., Polidori, D., Reichstein, M., Ribeca, A., van Ingen, C., Vuichard, N., Zhang, L., Amiro, B., Ammann, C., Arain, M. A., Ardö, J., Arkebauer, T., Arndt, S. K., Arriga, N., Aubinet, M., Aurela, M., Baldocchi, D., Barr, A., Beamesderfer, E., Marchesini, L. B., Bergeron, O., Beringer, J., Bernhofer, C., Berveiller, D., Billesbach, D., Black, T. A., Blanken, P. D., Bohrer, G., Boike, J., Bolstad, P. V., Bonal, D., Bonnefond, J.-M., Bowling, D. R., Bracho, R., Brodeur, J.,
- Brümmer, C., Buchmann, N., Burban, B., Burns, S. P., Buysse, P., Cale, P., Cavagna, M., Cellier, P., Chen, S., Chini, I., Christensen, T. R., Cleverly, J., Collalti, A., Consalvo, C., Cook, B. D., Cook, D., Coursolle, C., Cremonese, E., Curtis, P. S., D'Andrea, E., da Rocha, H., Dai, X., Davis, K. J., Cinti, B. D., Grandcourt, A. de, Ligne, A. D., De Oliveira, R. C., Delpierre, N., Desai, A. R., Di Bella, C. M., Tommasi, P. di, Dolman, H., Domingo, F., Dong, G., Dore, S., Duce, P., Dufrêne, E., Dunn, A., Dušek, J., Eamus, D., Eichelmann, U., ElKhidir, H. A. M., Eugster, W., Ewenz, C. M., Ewers, B., Famulari, D., Fares, S.,
- Feigenwinter, I., Feitz, A., Fensholt, R., Filippa, G., Fischer, M., Frank, J., Galvagno, M., et al.: The FLUXNET2015 dataset and the ONEFlux processing pipeline for eddy covariance data, Sci Data, 7, 225, https://doi.org/10.1038/s41597-020-0534-3, 2020.
- Plauborg, F., Abrahamsen, P., Gjettermann, B., Mollerup, M., Iversen, B. V., Liu, F., Andersen, M. N., and Hansen, S.: Modelling of root ABA synthesis, stomatal conductance, transpiration and potato production under water saving irrigation regimes, Agricultural Water Management, 98, 425–439, https://doi.org/10.1016/j.agwat.2010.10.006, 2010.





- de Pury, D. G. G. and Farquhar, G. D.: Simple scaling of photosynthesis from leaves to canopies without the errors of big-leaf models, Plant Cell Environ, 20, 537–557, https://doi.org/10.1111/j.1365-3040.1997.00094.x, 1997.
- Revill, A., Emmel, C., D'Odorico, P., Buchmann, N., Hörtnagl, L., and Eugster, W.: Estimating cropland carbon fluxes: A process-based model evaluation at a Swiss crop-rotation site, Field Crops Research, 234, 95–106, https://doi.org/10.1016/j.fcr.2019.02.006, 2019.
- Ridley, B., Boland, J., and Lauret, P.: Modelling of diffuse solar fraction with multiple predictors, Renewable Energy, 35, 478–483, https://doi.org/10.1016/j.renene.2009.07.018, 2010.
- Sabot, M. E. B., De Kauwe, M. G., Pitman, A. J., Medlyn, B. E., Ellsworth, D. S., Martin-StPaul, N. K., Wu, J., Choat, B., Limousin, J., Mitchell, P. J., Rogers, A., and Serbin, S. P.: One Stomatal Model to Rule Them All? Toward Improved
- Representation of Carbon and Water Exchange in Global Models, J Adv Model Earth Syst, 14, e2021MS002761, https://doi.org/10.1029/2021MS002761, 2022.
 - Sack, L. and Holbrook, N. M.: Leaf Hydraulics, Annu. Rev. Plant Biol., 57, 361–381, https://doi.org/10.1146/annurev.arplant.56.032604.144141, 2006.
- Schoups, G., Hopmans, J. W., Young, C. A., Vrugt, J. A., and Wallender, W. W.: Multi-criteria optimization of a regional spatially-distributed subsurface water flow model, Journal of Hydrology, 311, 20–48, https://doi.org/10.1016/j.jhydrol.2005.01.001, 2005.
 - Schulz, J.-P. and Vogel, G.: Improving the Processes in the Land Surface Scheme TERRA: Bare Soil Evaporation and Skin Temperature, Atmosphere, 11, 513, https://doi.org/10.3390/atmos11050513, 2020.
- Scott, R. L. and Biederman, J. A.: Partitioning evapotranspiration using long-term carbon dioxide and water vapor fluxes, Geophysical Research Letters, 44, 6833–6840, https://doi.org/10.1002/2017GL074324, 2017.
 - Senapati, N., Chabbi, A., and Smith, P.: Modelling daily to seasonal carbon fluxes and annual net ecosystem carbon balance of cereal grain-cropland using DailyDayCent: A model data comparison, Agriculture, Ecosystems & Environment, 252, 159–177, https://doi.org/10.1016/j.agee.2017.10.003, 2018.
- Shang, K., Ishibuchi, H., He, L., and Pang, L. M.: A Survey on the Hypervolume Indicator in Evolutionary Multiobjective Optimization, IEEE Trans. Evol. Computat., 25, 1–20, https://doi.org/10.1109/TEVC.2020.3013290, 2021.
 - Sharma, S. and Kumar, V.: A Comprehensive Review on Multi-objective Optimization Techniques: Past, Present and Future, Arch Computat Methods Eng, 29, 5605–5633, https://doi.org/10.1007/s11831-022-09778-9, 2022.
 - Sierra, M. R. and Coello Coello, C. A.: Improving PSO-Based Multi-objective Optimization Using Crowding, Mutation and €-Dominance, in: Evolutionary Multi-Criterion Optimization, vol. 3410, edited by: Coello Coello, C. A., Hernández Aguirre,
- 690 A., and Zitzler, E., Springer Berlin Heidelberg, Berlin, Heidelberg, 505–519, https://doi.org/10.1007/978-3-540-31880-4_35, 2005.
 - Stoy, P. C., El-Madany, T. S., Fisher, J. B., Gentine, P., Gerken, T., Good, S. P., Klosterhalfen, A., Liu, S., Miralles, D. G., Perez-Priego, O., Rigden, A. J., Skaggs, T. H., Wohlfahrt, G., Anderson, R. G., Coenders-Gerrits, A. M. J., Jung, M., Maes, W. H., Mammarella, I., Mauder, M., Migliavacca, M., Nelson, J. A., Poyatos, R., Reichstein, M., Scott, R. L., and Wolf, S.:





- Reviews and syntheses: Turning the challenges of partitioning ecosystem evaporation and transpiration into opportunities, Biogeosciences, 16, 3747–3775, https://doi.org/10.5194/bg-16-3747-2019, 2019.
 - Suleau, M., Moureaux, C., Dufranne, D., Buysse, P., Bodson, B., Destain, J.-P., Heinesch, B., Debacq, A., and Aubinet, M.: Respiration of three Belgian crops: Partitioning of total ecosystem respiration in its heterotrophic, above- and below-ground autotrophic components, Agricultural and Forest Meteorology, 151, 633–643, https://doi.org/10.1016/j.agrformet.2011.01.012, 2011.
 - Swenson, S. C. and Lawrence, D. M.: Assessing a dry surface layer-based soil resistance parameterization for the Community Land Model using GRACE and FLUXNET-MTE data, JGR Atmospheres, 119, https://doi.org/10.1002/2014JD022314, 2014. Tang, Y., Marshall, L., Sharma, A., and Ajami, H.: A Bayesian alternative for multi-objective ecohydrological model specification, Journal of Hydrology, 556, 25–38, https://doi.org/10.1016/j.jhydrol.2017.07.040, 2018.
- Tenreiro, T. R., García-Vila, M., Gómez, J. A., Jimenez-Berni, J. A., and Fereres, E.: Water modelling approaches and opportunities to simulate spatial water variations at crop field level, Agricultural Water Management, 240, 106254, https://doi.org/10.1016/j.agwat.2020.106254, 2020.
 - Timlin, D., Paff, K., and Han, E.: The role of crop simulation modeling in assessing potential climate change impacts, Agrosystems Geosci & Env, 7, e20453, https://doi.org/10.1002/agg2.20453, 2024.
- Urban, J., Ingwers, M., McGuire, M. A., and Teskey, R. O.: Stomatal conductance increases with rising temperature, Plant Signaling & Behavior, 12, e1356534, https://doi.org/10.1080/15592324.2017.1356534, 2017.
 - Van Den Hoof, C., Hanert, E., and Vidale, P. L.: Simulating dynamic crop growth with an adapted land surface model JULES-SUCROS: Model development and validation, Agricultural and Forest Meteorology, 151, 137–153, https://doi.org/10.1016/j.agrformet.2010.09.011, 2011.
- Wang, B., Yan, H., Zheng, H., Wu, J., Tian, D., Zhang, C., Zhu, X., Wang, G., Lakhiar, I. A., and Liu, Y.: Estimation of latent heat flux of pasture and maize in arid region of Northwest China based on canopy resistance modeling, Front. Environ. Sci., 12, 1397704, https://doi.org/10.3389/fenvs.2024.1397704, 2024.
 - Wöhling, T., Gayler, S., Priesack, E., Ingwersen, J., Wizemann, H.-D., Högy, P., Cuntz, M., Attinger, S., Wulfmeyer, V., and Streck, T.: Multiresponse, multiobjective calibration as a diagnostic tool to compare accuracy and structural limitations of five
- coupled soil-plant models and CLM3.5: MULTIOBJECTIVE CALIBRATION AS DIAGNOSTIC TOOL, Water Resour. Res., 49, 8200–8221, https://doi.org/10.1002/2013WR014536, 2013.
 - Yin, X., Kersebaum, K.-C., Beaudoin, N., Constantin, J., Chen, F., Louarn, G., Manevski, K., Hoffmann, M., Kollas, C., Armas-Herrera, C. M., Baby, S., Bindi, M., Dibari, C., Ferchaud, F., Ferrise, R., De Cortazar-Atauri, I. G., Launay, M., Mary, B., Moriondo, M., Öztürk, I., Ruget, F., Sharif, B., Wachter-Ripoche, D., and Olesen, J. E.: Uncertainties in simulating N
- uptake, net N mineralization, soil mineral N and N leaching in European crop rotations using process-based models, Field Crops Research, 255, 107863, https://doi.org/10.1016/j.fcr.2020.107863, 2020.
 - Yin, X. and van Laar, H. H.: Crop Systems Dynamics: An ecophysiological simulation model of genotype-by-environment interactions, Brill | Wageningen Academic, https://doi.org/10.3920/978-90-8686-539-0, 2005.





Zhang, Y., Arabi, M., and Paustian, K.: Analysis of parameter uncertainty in model simulations of irrigated and rainfed agroecosystems, Environmental Modelling & Software, 126, 104642, https://doi.org/10.1016/j.envsoft.2020.104642, 2020. Zhou, H., Zhou, G., He, Q., Zhou, L., Ji, Y., and Zhou, M.: Environmental explanation of maize specific leaf area under varying water stress regimes, Environmental and Experimental Botany, 171, 103932, https://doi.org/10.1016/j.envexpbot.2019.103932, 2020.

Zhou, S., Duursma, R. A., Medlyn, B. E., Kelly, J. W. G., and Prentice, I. C.: How should we model plant responses to drought?

An analysis of stomatal and non-stomatal responses to water stress, Agricultural and Forest Meteorology, 182–183, 204–214,
https://doi.org/10.1016/j.agrformet.2013.05.009, 2013.